JACS
JOURNAL OF THE AMERICAN CHEMICAL SOCIETY
Article
pubs.acs.org/JACS

A Paradigmatic Change: Linking Fullerenes to Electron Acceptors

Lai Feng,[†,‡] Marc Rudolf,[§] Silke Wolfrum,[§] Anna Troeger,[§] Zdenek Slanina,[‡] Takeshi Akasaka,*[,‡] Shigeru Nagase,[#] Nazario Martín,[∥] Tayebeh Ameri,[⊥] Christoph J. Brabec,[⊥] and Dirk M. Guldi*[,§]

[†]School of Energy, Soochow University, Suzhou 215006, P.R. China

[‡]Life Science Center of Tsukuba Advanced Research Alliance, University of Tsukuba, Tsukuba 305-8577, Japan

[§]Department of Chemistry and Pharmacy and Interdisciplinary Center for Molecular Materials, Friedrich-Alexander-Universität Erlangen-Nürnberg, 91058 Erlangen, Germany

[#]Fukui Institute for Fundamental Chemistry, University of Kyoto, Kyoto 606-8103, Japan

[∥]Departamento de Química Orgánica, Facultad de Química, Universidad Complutense, E-28040 Madrid, Spain, and IMDEA-Nanociencia, Campus de Cantoblanco, E-28049 Madrid, Spain

[⊥]I-MEET (WW6), Friedrich-Alexander-Universität Erlangen-Nürnberg, Martensstraße 7, 91058 Erlangen, Germany

Supporting Information

ABSTRACT: The potential of $Lu_3N@C_{80}$ and its analogues as electron acceptors in the areas of photovoltaics and artificial photosynthesis is tremendous. To this date, their electron-donating properties have never been explored, despite the facile oxidations that they reveal when compared to those of C_{60}. Herein, we report on the synthesis and physicochemical studies of a covalently linked $Lu_3N@C_{80}$–perylenebisimide (PDI) conjugate, in which PDI acts as the light harvester and the electron acceptor. Most important is the unambiguous evidence—in terms of spectroscopy and kinetics—that corroborates a photoinduced electron transfer evolving from the ground state of $Lu_3N@C_{80}$ to the singlet excited state of PDI. In stark contrast, the photoreactivity of a C_{60}–PDI conjugate is exclusively governed by a cascade of energy-transfer processes. Also, the electron-donating property of the $Lu_3N@C_{80}$ moiety was confirmed through constructing and testing a bilayer heterojunction solar cell device with a PDI and $Lu_3N@C_{80}$ derivative as electron acceptor and electron donor, respectively. In particular, a positive photovoltage of 0.46 V and a negative short circuit current density of 0.38 mA are observed with PDI/Ca as anode and ITO/$Lu_3N@C_{80}$ as cathode. Although the devices were not optimized, the sign of the V_{OC} and the flow direction of J_{SC} clearly underline the unique oxidative role of $Lu_3N@C_{80}$ within electron donor–acceptor conjugates toward the construction of novel optoelectronic devices.

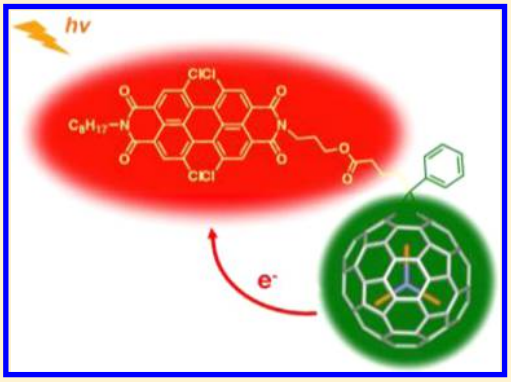

INTRODUCTION

Empty fullerenes such as C_{60} and C_{70} are spherical building blocks of nanometer dimensions and have been widely used as electron acceptors[1,2] in artificial photosynthesis and photovoltaics because of their excellent electrochemical and photophysical properties.[3] However, in contrast to its nice electron-accepting property, the electron-donating property of C_{60} is very poor, which relates primarily to its high oxidation potential of 1.26 V vs that of ferrocene/ferricenium ($Fc^{0/+}$).[4] In fact, the electron transfer oxidation of C_{60} only occurs with the help of either strong oxidants/acceptors or scandium ions that can bind with the electron transfer product.[5] Such limitations impede, however, its application as a widely applicable electron donor.

Endohedral metallofullerenes (EMFs) are types of special fullerene derivatives. Their unique physicochemical properties and rich electrochemical properties, in particular, relate to a significant hybridization effect of the encapsulated metallic cluster.[6,7] Recently, a variety of EMFs have been integrated into various photoactive conjugates or hybrids, and these EMFs reveal their distinctive photophysical behaviors.[7a,8] Some of them, especially nitride cluster fullerenes (NCFs) such as $M_3N@C_{2n}$, have been found to be superior electron acceptors when compared to C_{60}.[9] Still, electron transfer oxidations of NCFs have been seldom probed,[10] despite the fact that their one-electron oxidation potentials are generally much lower than those found in C_{60}. Specifically, the oxidation potential of $Lu_3N@C_{80}$ is 0.62 V lower than that of C_{60}. Therefore, we postulate its better electron donor properties and easier photoinduced electron transfer oxidations. For further confirmation, herein, we attach an electron acceptor to $Lu_3N@C_{80}$, which is aiming to power a photoinduced electron transfer oxidation of $Lu_3N@C_{80}$. In particular, a perylene dye, namely 1,6,7,12-tetrachloro-3,4,9,10-perylenediimide (PDI), is used as electron acceptor due to its outstanding light-harvesting and electron-accepting features.[11] Importantly, a photoinduced

Received: April 25, 2012
Published: June 11, 2012

   dx.doi.org/10.1021/ja3039695 | J. Am. Chem. Soc. 2012, 134, 12190–12197

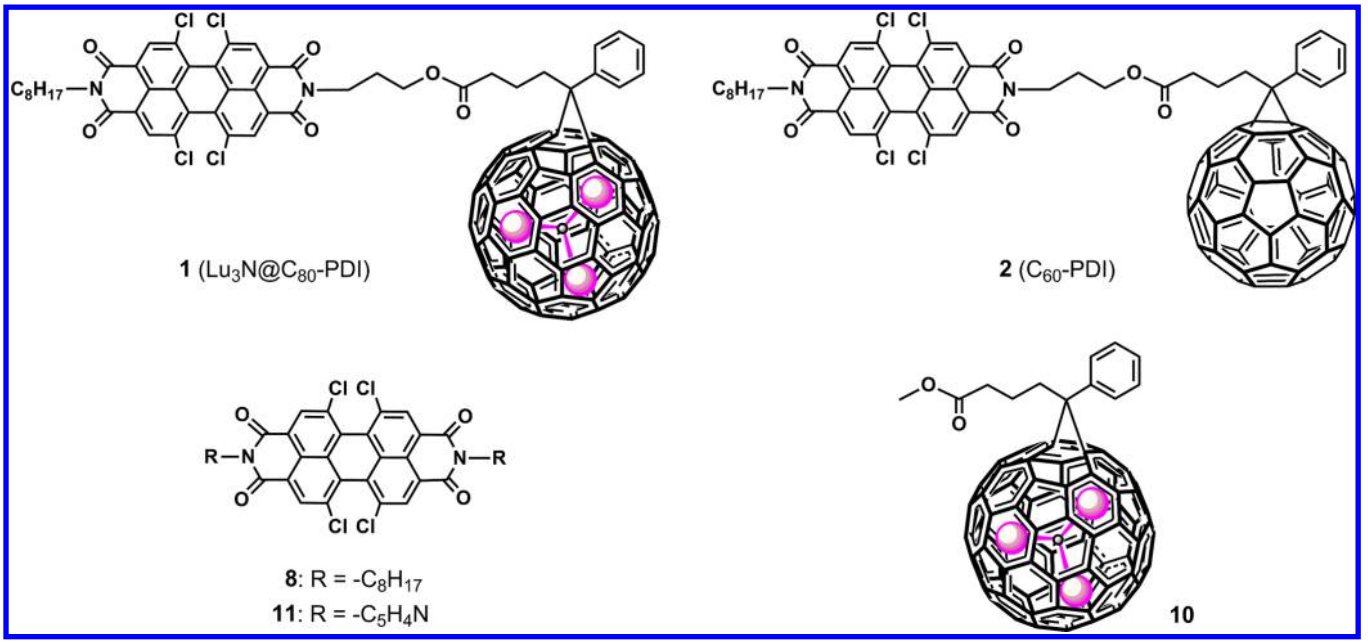

Figure 1. Schematic structures of conjugates **1** and **2** as well as those for compounds **8**, **10**, **11**.

electron transfer oxidation of $Lu_3N@C_{80}$ is identified in the physicochemical studies of the $Lu_3N@C_{80}$–PDI conjugate (**1**) (see Figure 1), which is in contrast to the analogues C_{60}–PDI conjugate (**2**). Also, we further explored the electron-donating potential of $Lu_3N@C_{80}$ derivatives in a photovoltaic device.

RESULTS AND DISCUSSION

The syntheses of **1** and **2** were carried out via [1 + 2]-cycloaddition reaction of PDI diazo compounds, which were generated in situ by a Bamford–Stevens reaction between PDI tosylhydrazone (**9**) and sodium methoxide (Schemes S1–S3, Supporting Information). In fact, the thermal reaction of C_{60} with **9** gave rise to the [6,6]-closed (**2**) and [5,6]-open (**3**) isomers of C_{60}–PDI, while only the [6,6]-open isomer (**1**) of $Lu_3N@C_{80}$–PDI was found in the reaction with $Lu_3N@C_{80}$. All of the compounds were isolated and purified by HPLC. However, only **1** and **2** were thermodynamically stable and, thus, further studied.

MALDI-TOF mass and NMR experiments—see Supporting Information—served as the basis for the structural characterization of **1** and **2**. The mass spectra of **1** in positive and negative modes show distinct peaks at m/z of 2358 and 2356 that are respectively assigned to the $[\mathbf{1} + 2H]^{2+}$ and $[\mathbf{1}]^-$ ions, whereas the mass peak of **2** at m/z of 1576 is only observed in negative mode. The ^{1}H NMR spectra of **1** and **2** reveal the signals for the perylene moiety at around 8.6 ppm together with the aromatic protons of the phenylmethane moiety and the protons of the alkyl chains. In the ^{13}C NMR spectra of **1**, the signals between 98 and 94 ppm are assigned to the bridgehead atoms, reflecting their sp^2 character due to the [6,6]-open addition pattern, which are quite different from those of **2** at 79 ppm. The signal at 51 ppm corresponds to the spiro carbon of **1** in analogy to that of **2**.

Figure 2 summarizes the absorption spectra of all of the PDI-containing compounds, that is, **1**, **2**, **8**, and **10**, at room temperature. Common to these spectra are features at 430, 487–490, and 522–524 nm. In addition, in **1** the $Lu_3N@C_{80}$ features emerge at 405 and 675 nm, while in **2** the features at 330, 433, and 695 nm are C_{60} centered. However, the

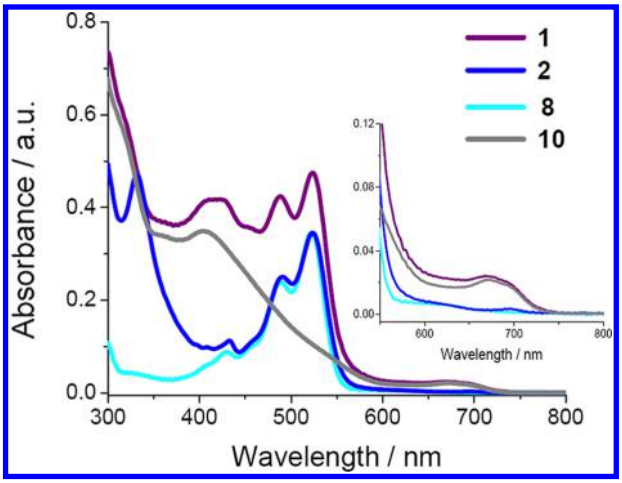

Figure 2. UV–vis absorption spectra of **1**, **2**, **8**, and **10** in toluene. Inset shows enlarged absorptions between 550 and 800 nm.

absorption spectrum of **1** differs slightly from the linear superimpositions of the individual components. Red shifts of the absorption maxima, which range from 1 to 3 nm (see Supporting Information, Figure S18), document the electronic communications/short intramolecular distances between PDI and $Lu_3N@C_{80}$.

The electrochemical properties of **1** and **2** were investigated by means of differential pulse voltammetry (DPV) and cyclic voltammetry (CV) (Table 1, Figures S19 and S20, see Supporting Information). Using **8** and **10** as references allows for the accurate assignment of the individual redox steps. **1** shows in the cathodic direction four one-electron reduction steps. The first and second reductions (i.e., −0.86 and −1.08 V) are assigned to the formation of the π-radical anion of PDI and the dianion of PDI, respectively. The third and forth reductions (i.e., −1.41 and −1.87 V) relate to $Lu_3N@C_{80}$ centered processes. In the anodic direction, only an one-electron oxidation step is observed for **1**. This oxidation (i.e., +0.57 V) is due to the formation of the π-radical cation of $Lu_3N@C_{80}$.

dx.doi.org/10.1021/ja3039695 | J. Am. Chem. Soc. 2012, 134, 12190–12197

Table 1. Redox Potentials of PDI–Fullerene Conjugates 1, 2, and Reference Compounds[a]

	E_1^{ox}	E_1^{red}	E_2^{red}	E_3^{red}	E_4^{red}
1	0.57[b]	−0.86	−1.08	−1.41[b]	−1.87
2	1.21	−0.89	−1.13	−1.52	
8		−0.89	−1.12		
10	0.55[b]	−1.46[b]	−1.94		

[a]All the potentials, in volts, were measured relative to the Fc/Fc^+ couple by means of DPV. [b]Quasi-reversible process determined via CV.

For **2**, three one-electron reduction steps emerge in the cathodic direction. In particular, reductions at −0.89, −1.13, and −1.52 V correspond to the formation of the PDI π-radical anion, the PDI dianion/C_{60} π-radical anion and the C_{60} dianion, respectively. In the anodic direction, the π-radical cation formation of C_{60} sets in at +1.21 V for **2**. The fact that the one-electron reduction and the one-electron oxidation of **1** differ slightly from those seen for **8** (i.e., −0.89 V) and **10** (+0.55 V), respectively, points to appreciable ground state interactions between PDI and $Lu_3N@C_{80}$. In **2**, on the other hand, no particular differences were noted.

Next, the structures of **1** and **2** were optimized using DFT method at the M06-2X[12]/3-21G~SDD level[13,14] with a Gaussian 09 package,[15] and the corresponding energy-minimum conformers are shown in Figure S23 (see Supporting Information). Common is the close proximity between PDI and $Lu_3N@C_{80}$ or C_{60}. Shortest intramolecular distances of around 2.8 Å are indicative for significant through-space interactions. In addition, **1** and **2** reveal similar MO distributions (Figure 3) that is, localization of the HOMO on

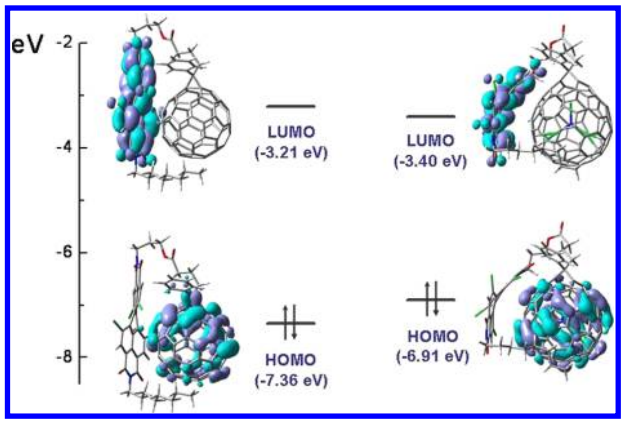

Figure 3. MO diagram of **1** (right) and **2** (left).

$Lu_3N@C_{80}$ or C_{60} and that of the LUMO on PDI. Upon closer inspection, the calculated MOs agree well with the electrochemistry data. In particular, a HOMO, which is 0.45 eV higher in **1** than in **2**, relates to the easier oxidation of $Lu_3N@C_{80}$ relative to C_{60}. The LUMO of **1**, on the other hand, is 0.19 eV lower than that of **2**, reflecting a slightly easier PDI reduction in **1** as compared to that in **2**. Implicit is a redistribution of electron density, that is, from $Lu_3N@C_{80}$ to PDI.

To attribute our spectral observation (vide infra) spectroelectrochemical experiments, that is, the formation of the PDI π-radical anion and $Lu_3N@C_{80}$ π-radical cation, were deemed necessary. Spectroelectrochemical experiments were performed in either deaerated toluene/acetonitrile mixtures (4:1 v/v) or in deaerated *o*-DCB. The differential absorption spectrum following the conclusion of the spectroelectrochemical reduction of PDI is shown in Figure 4. Sets of maxima at

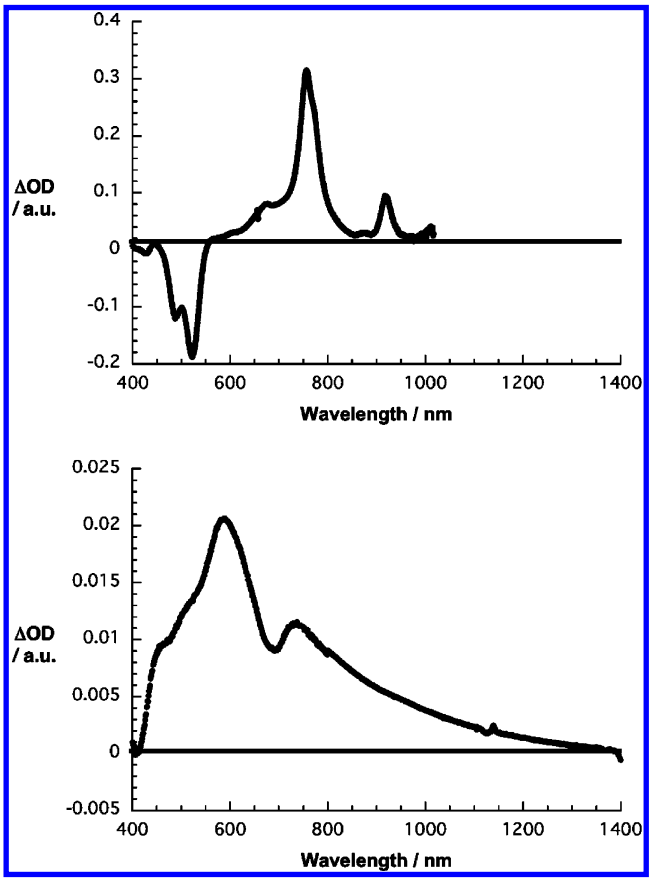

Figure 4. (Top) Differential absorption spectra (visible and near-infrared) obtained upon electrochemical reduction of **8** at an applied bias of −0.7 V in argon-saturated toluene/acetonitrile mixtures (4/1 v/v) at room temperature. (Bottom) Differential absorption spectra (visible and near-infrared) obtained upon electrochemical oxidation of **10** at an applied bias of +0.6 V in argon-saturated *o*-dichlorobenzene at room temperature.

444, 675, 756, and 918 nm as well as minima at 489 and 522 nm are formed under pseudo-first-order conditions. On the other hand, $Lu_3N@C_{80}$ oxidation experiments led to differential absorption changes that include maxima at 585 and 730 nm and a broad tail that reaches out into the near-infrared.

Fluorescence assays with **1**, **2**, and **8** disclose a rather strong fluorescence quenching in the earlier two. The fluorescence quantum yields were 0.91 (toluene, chlorobenzene, benzonitrile) for **8**, 0.045 (toluene), 0.038 (chlorobenzene), 0.033 (benzonitrile) for **2**, and 0.017 (toluene), 0.015 (chlorobenzene), 0.014 (benzonitrile) for **1**. Notably, the weak fluorescent features of C_{60} and $Lu_3N@C_{80}$ with quantum yields of less than 10^{-4} hamper any meaningful analysis. In conclusion, we postulate a rapid PDI excited state deactivation in **1** and **2**.

Decisive insights into the excited state deactivation of PDI in **1** and **2**, in general, and into the corresponding photoproducts, in particular, came from transient absorption measurements. To this end, **8** reveals upon femtosecond excitation at 530 nm differential absorption changes that include transient maxima at 755, 800, 875, and 970 nm as well as transient minima at 490 and 515 nm—Figure 5. These features relate to the singlet–singlet transitions of photoexcited PDI, which decay with a

dx.doi.org/10.1021/ja3039695 | J. Am. Chem. Soc. 2012, 134, 12190–12197

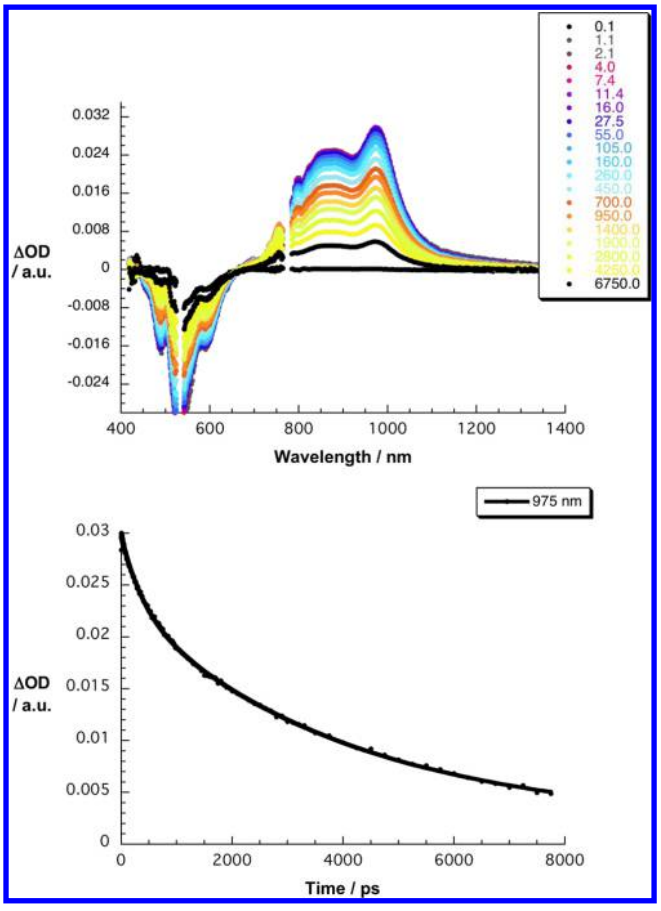

Figure 5. (Top) Differential absorption spectra (visible and near-infrared) obtained upon femtosecond flash photolysis (530 nm) of **8** (3.7×10^{-5} M) in argon-saturated chlorobenzene with several time delays between 0 and 6750 ps at room temperature. (Bottom) Time–absorption profiles of the spectra shown above at 975 nm monitoring the excited state decay.

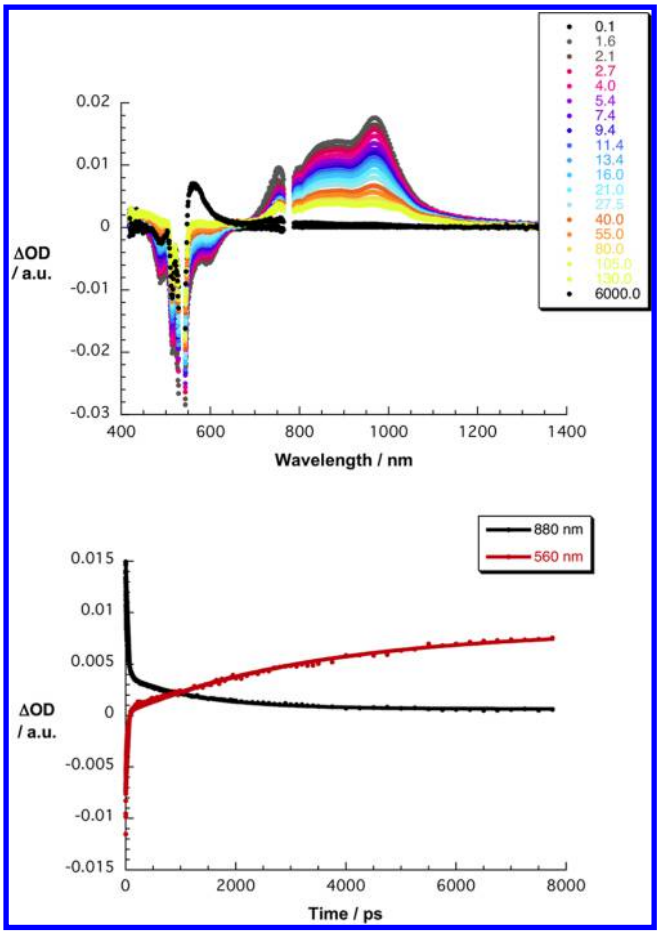

Figure 6. (Top) Differential absorption spectra (visible and near-infrared) obtained upon femtosecond flash photolysis (530 nm) of **2** (3.7×10^{-5} M) in argon saturated chlorobenzene with several time delays between 0 and 6000 ps at room temperature. (Bottom) Time–absorption profiles of the spectra shown above at 560 and 880 nm monitoring the energy transfer reactions.

lifetime of 4.0 ± 0.2 ns. It is, however, the ground state rather than the triplet excited state that is populated due to an inefficient intersystem crossing.[16] In addition, a minimum evolves in the range of no ground state absorption, that is, at 595 nm.[17] Complementary nanosecond excitation at 532 nm further corroborates the spin-allowed ground state recovery, that is, the lack of an appreciable transient (not shown).

Excitation of **2** at 530 nm results in the exclusive formation of the PDI singlet excited state. Notable is the light partition of C_{60} vs PDI at the excitation wavelength (1:24). Transient maxima at 755, 790, 880, and 970 nm as well as transient minima at 490 and 515 nm are formed instantaneously despite the presence of C_{60}—Figure 6. However, the presence of C_{60} exerts an impact on the PDI singlet excited state lifetime, namely a rapid decay with an underlying lifetime of 35 ± 5 ps. At the conclusion of this decay, only a broad feature around 880 nm remains discernible in the near-infrared region of the spectrum. In the visible region, which is initially dominated by the ground state bleaching of PDI, an additional band is noticeable at 460 nm. Owing to the similarity of the aforementioned features (i.e., 460 and 880 nm) with those known for the C_{60} singlet excited state and the exclusive excitation of PDI at 530 nm we postulate an exothermic transduction of singlet excited state energy. In most C_{60} derivatives, the deactivation of the C_{60} singlet excited state is dominated by intersystem crossing (1.5 ± 0.1 ns) to the energetically lower-lying triplet excited state. In this regard, it is important to note that in **2**, the 880 nm transition decays with kinetics that are hardly faster (1.4 ± 0.1 ns) than the inherent intersystem crossing dynamics of C_{60}. Interestingly, we did not find the characteristic C_{60} triplet feature—a strong triplet–triplet transition at 700 nm with an extinction coefficient of ~15.000 M^{-1} cm^{-1}—at the end of the C_{60} singlet excited state deactivation.[3c] On the contrary, minima at 490 and 515 nm as well as a maximum at 565 nm were concluded. Earlier we have established that such features are reliable attributes of the PDI triplet excited state.[18] From this we infer that the C_{60} triplet (1.5 eV), once formed, undergoes a thermodynamically allowed transfer of triplet excited state energy to PDI (1.2 eV). Nearly, similar kinetics at the 565 nm maximum (1.4 ± 0.1 ns), which allowed us to follow the generation of the PDI triplet excited state, further furnishes the following kinetic assignment—the rate-determining step in the PDI triplet excited state formation is the C_{60} centered intersystem crossing. The only component seen in the complementary nanosecond experiments—following 532 nm excitation—was that of the PDI triplet formed with quantum yields of 0.52 and 1.0 in toluene and chlorobenzene as inferred from singlet oxygen quantum yields—Figure S24 in Supporting Information.

dx.doi.org/10.1021/ja3039695 | J. Am. Chem. Soc. 2012, 134, 12190–12197

Exciting **2** at 387 nm forms the singlet excited state of C_{60} directly. The latter undergoes intersystem crossing to the corresponding triplet excited state. Nevertheless, the differential absorption changes that are recorded at the end of the intersystem crossing process resemble those of the PDI triplet excited state. Most notable are the 565 nm maximum the 480/525 nm minima seen at time delays of about 4 ns and beyond—Figure S25 (Supporting Information). Such an observation is in line with the sequence of a slow intersystem crossing and a fast triplet−triplet energy transfer.

When **1** was examined subsequent to laser excitation at 530 nm, the same singlet excited state features, which were observed in the cases of **2** and **8**, developed at the conclusion of the laser excitation—Figure 7. This, again, attests to the successful PDI excitation. However, instead of seeing the slow intersystem crossings, the PDI singlet excited state decays ultrafast with lifetimes less than 1.0 ps (see Figure 7). Simultaneously with the latter decay, new transitions grow-in in the visible, namely maxima around 575, 700, 760, and 890 nm, and in the near-infrared, namely a broad near-infrared tail. On the basis of a spectral comparison—vide infra—we ascribe the visible bands to the PDI π-radical anion ($PDI^{\bullet-}$), while the near-infrared band corresponds to the $Lu_3N@C_{80}$ π-radical cation $[(Lu_3N@C_{80})^{\bullet+}]$. In accordance with these results, we propose that in **1** electron transfer evolves from the electron-donating $Lu_3N@C_{80}$ to the PDI singlet excited state to yield $(Lu_3N@C_{80})^{\bullet+}-PDI^{\bullet-}$ for which we estimate, on the basis of electrochemical data, an energy of 1.43 eV. Notably, $(Lu_3N@C_{80})^{\bullet+}-PDI^{\bullet-}$ is metastable and decays with a lifetime of 120 ± 10 ps in toluene, 100 ± 10 ps in chlorobenzene and 45 ± 5 ps in benzonitrile. For **1**, the PDI triplet excited state emerges as the product of charge recombination. Again, in complementary nanosecond experiments—following 532 nm excitation—the only product that was monitored was that of the PDI triplet—Figure S26. As singlet oxygen quantum yields suggest, the triplet is formed with quantum yields of 0.58, 0.97, and 0.23 in toluene, chlorobenzene, and benzonitrile, respectively.

In contrast to the aforementioned, 387 nm photoexcitation of **1** generates the relatively short-lived (50 ± 2 ps) singlet excited state of **1**. However, its energy (1.70 eV) is insufficient to power the electron transfer that has been seen to evolve from the PDI singlet excited state. As a matter of fact, the corresponding triplet excited state fingerprint at 570 nm develops and remains stable on the experimental time scale of our setup, that is, 8 ns. All of the different electron- and energy-transfer pathways occurring upon photoexcitation of **1** or **2** are summarized in energy diagrams: see Figure 8.

To further corroborate the photoinduced oxidation of $Lu_3N@C_{80}$ in the presence of the electron-accepting PDI, bilayer-structured solar cell devices were prepared by utilizing, in contrast to previous studies,[9c] **10** as an electron donor and a tetrachlorinated perylenebisimide derivative—(1,6,7,12-tetrachloro-*N*,*N*′-di(4-pyridyl)-perylene-3,4,9,10-tetracarboxylic diimide)[19] (**11**)—as an electron acceptor. The fabricated devices had the following configurations: indium tin oxide (ITO)/poly(3,4-ethylenedioxythiophene:polystyrene sulfonate) (PEDOT:PSS) (50 nm)/**10** (30 nm)/**11** (40 nm)/Ca (15 nm)/Ag (80 nm). Doctor blading was employed for depositing the hole-transporting PEDOT:PSS and the electron-donating layer of **10**, whereas the electron-accepting layer constituted by **11** as well as the Ca/Ag cathode were deposited by thermal evaporation followed by postannealing. Figure 9 shows the current density (J) vs voltage (V) curves under illumination and

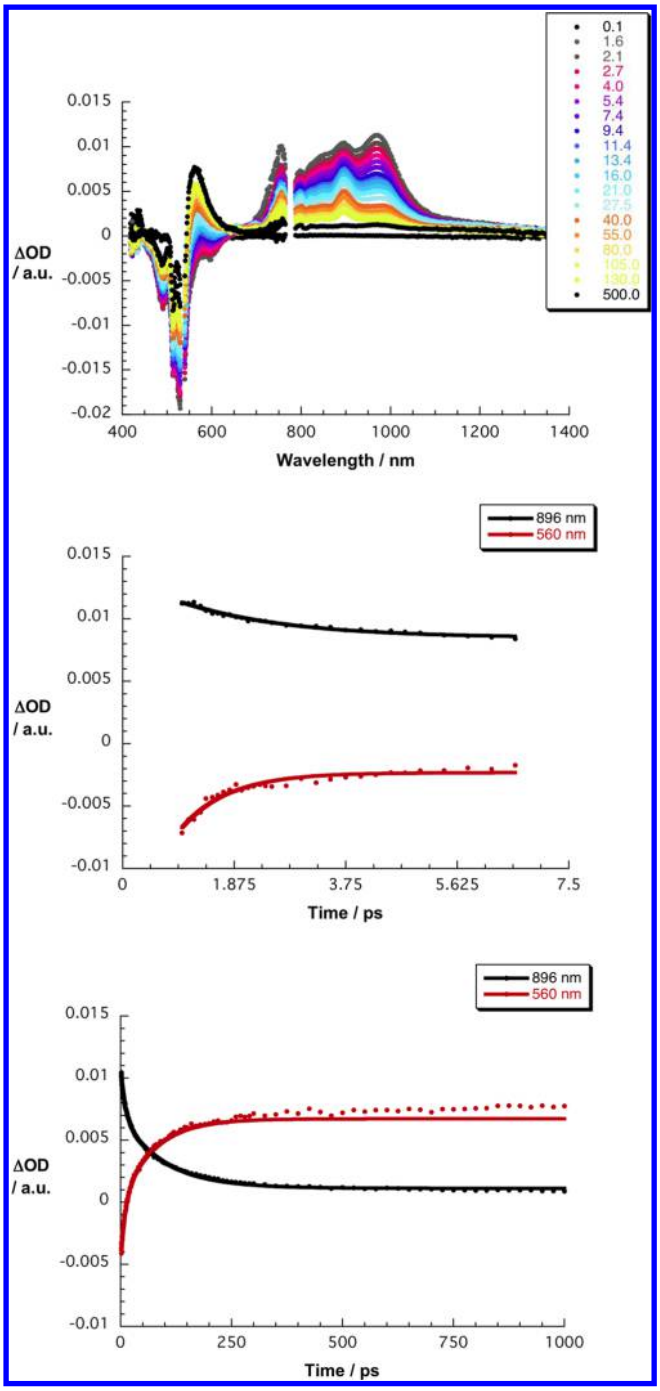

Figure 7. (Top) Differential absorption spectra (visible and near-infrared) obtained upon femtosecond flash photolysis (530 nm) of **1** (3.7×10^{-5} M) in argon-saturated chlorobenzene with several time delays between 0 and 500 ps at room temperature. (Middle) Time−absorption profiles of the spectra shown above at 560 and 896 nm monitoring the charge separation. (Bottom) Time−absorption profiles of the spectra shown above at 560 and 896 nm monitoring the charge recombination.

in the dark for a **10**/**11** device. Under simulated 1 sun AM 1.5G radiation (100 mW/cm^2), a short circuit current density (J_{SC}) of 0.38 mA, an open circuit voltage (V_{OC}) of 0.46 V, a fill factor (FF) of 30.24%, and an efficiency (η) of 0.054% were determined. It is important to note that the devices were not optimized in terms of layer thicknesses or thermal annealing conditions. Nevertheless, our preliminary results clearly under-

dx.doi.org/10.1021/ja3039695 | J. Am. Chem. Soc. 2012, 134, 12190−12197

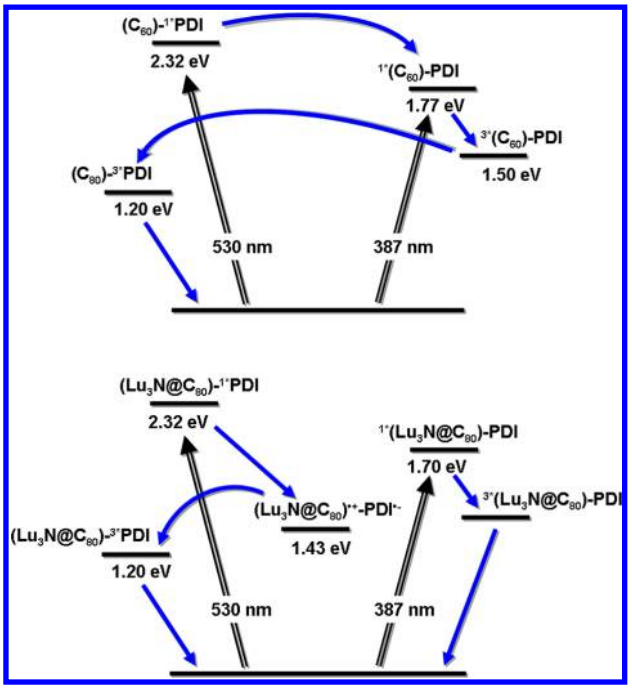

Figure 8. (Top) Energy level diagram of **2** (C_{60}–PDI) and (bottom) energy diagram level of **1** ($Lu_3N@C_{80}$–PDI), reflecting the different pathways of energy and electron transfer.

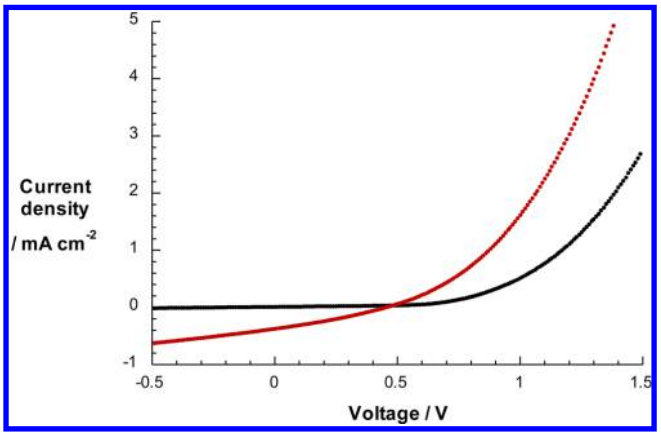

Figure 9. Current density–voltage (J–V) characteristics—a short circuit current density (J_{SC}) of 0.38 mA, an open circuit voltage (V_{OC}) of 0.46 V, a fill factor (FF) of 30.24%, and an efficiency (η) of 0.054%—under AM 1.5 radiation with the illuminated current density and dark current density shown as red and black lines, respectively.

line the proceeding charge transfer between $Lu_3N@C_{80}$ and PDI.

CONCLUSION

In conclusion, we have successfully designed, synthesized, and probed a covalently linked $Lu_3N@C_{80}$–PDI electron donor–acceptor conjugate. With the help of femtosecond transient absorption measurements we have unambiguously corroborated for the first time that a photoinduced electron transfer event evolves from the ground state of $Lu_3N@C_{80}$ to the excited state of PDI. This result is in stark contrast to the excited state deactivation of an analogue C_{60}–PDI electron donor–acceptor conjugate, in which the presence of two electron acceptors precludes any electron transfer at all. Instead, a cascade of energy transfer reactions shuttles the excited state energy back and forth between PDI and C_{60}. Overall, the facile oxidation of $Lu_3N@C_{80}$ is believed to be sufficient in driving this unprecedented electron transfer event. In preliminary assays, we have applied $Lu_3N@C_{80}$-PCBM (**10**) as an electron donor in a bilayer heterojunction solar cell device with PDI derivative (**11**) as electron acceptor. Although the overall efficiencies were rather moderate with values of 0.054% (i.e., under nonoptimized conditions) the electron-donating property of $Lu_3N@C_{80}$ was undoubtedly confirmed, that is, a positive photovoltage of 0.46 V and a negative short circuit current density of 0.38 mA with PDI/Ca as anode and ITO/$Lu_3N@C_{80}$ as cathode. This work, therefore, discloses a new way of using NCFs as electron donors toward the construction of optoelectronic devices integrating n-type semiconductors.

EXPERIMENTAL SECTION

Spectroscopy. All NMR spectra were recorded respectively on a Bruker AC 300 spectrometer or Bruker AV 500 spectrometer with a CryoProbe system, locked on deuterated solvents and referenced to the solvent peak. The 1D (^{1}H, ^{13}C and DEPT45/135) and 2D experiments (COSY and HMQC) were performed by means of standard experimental procedures of the Bruker library. Absorption spectra of all samples were recorded in toluene with a Shimadzu UV-3150 spectrometer using a quartz cell and 1-nm resolution. Matrix-assisted laser desorption–ionization time-of flight (MALDI-TOF) mass spectra were recorded with a Bruker BIFLEX-III mass spectrometer using 1,1,4,4-tetraphenyl-1,3-butadiene as the matrix. The measurements were performed in both positive and negative ion modes.

Steady-State Emission. The spectra were recorded on a FluoroMax 3 fluorometer (vis detection) and on a Fluorolog spectrometer (NIR detection). Both spectrometers were built by HORIBA JobinYvon. The measurements were carried out at room temperature under argon atmosphere.

Time Resolved Absorption. Femtosecond transient absorption studies were performed with 387 and 530 nm laser pulses (1 kHz, 150 fs pulse width) from an amplified Ti:Sapphire laser system (Clark-MXR, Inc.), the laser energy was 200 nJ. Nanosecond laser flash photolysis experiments were performed with (355 and) 532 nm laser pulse from a Quanta-Ray CDR Nd:YAG system (6 ns pulse width) in a front face excitation geometry.

Time Resolved Emission. Fluorescence lifetimes were measured by using a Fluorolog (Horiba Jobin Yvon).

Electrochemistry. Differential pulse voltammetry (DPV) and cyclic voltammetry (CV) were carried out in *o*-DCB using a BAS CW-50 instrument. A conventional three-electrode cell consisting of a platinum working electrode, a platinum counter-electrode, and a saturated calomel reference electrode (SCE) was used for both measurements. 0.05 M $(n\text{-Bu})_4NPF_6$ was used as the supporting electrolyte. All potentials were recorded against a SCE reference electrode and corrected against Fc/Fc^+. DPV and CV were measured at a scan rate of 20 and 50 mV s^{-1}, respectively.

Materials. All chemicals were of reagent grade and purchased from Wako. $Lu_3N@I_h$-C_{80} (>99%) was purchased from Luna Co.. Preparative and analysis HPLC were performed on semi preparative Buckyprep column (ø 10 × 100 mm, Cosmosil), semi-preparative 5PBB column (ø 10 mm × 100 mm, Cosmosil) and Buckyprep column and Buckyclutcher column (ø 4.6 mm × 100 mm, Cosmosil), respectively. Toluene was used as eluent.

Spectroelectrochemistry. The spectroelectrochemical measurements were done on a Varian Cary 5000 UV–vis–NIR spectrophotometer connected to a Princeton PGstat 263A using a home-made cell with three-electrode configuration. A light transparent platinum gauze, a platinum plate, and a silver wire were employed as the working, counter, and reference electrodes, respectively, in an analyte solution of *o*-dichlorobenzene containing 0.05 M tetrabutylammonium-hexafluorophosphate as supporting electrolyte.

dx.doi.org/10.1021/ja3039695 | J. Am. Chem. Soc. 2012, 134, 12190–12197

Synthesis of Conjugate 1. Compound **9** (7.5 mg, 7.2 μmol) and NaOMe (0.8 mg, 0.015 mmol) were dissolved in pyridine (0.5 mL) and stirred for 30 min at 65 °C under N_2. Then, $Lu_3N@C_{80}$ (1.5 mg, 1 μmol) in 2.5 mL *o*-DCB was added in. The mixture was stirred at 80 °C for 3 h under N_2. The reaction mixture was separated by HPLC (Buckyprep column, toluene); the second fraction is the dyad of $Lu_3N@C_{80}$−PDI (**1**). **1** was further purified by Buckyprep column. Yield: 1.0 mg, 46% based on consumed $Lu_3N@C_{80}$; ^{1}H NMR (500 MHz, $C_2D_4Cl_2$): δ 8.585 (s, 1H), 8.581 (s, 2H), 8.576 (s, 1H), 7.949 (br, 1H), 7.890 (d, ^2J = 7.4 Hz, 1H), 7.447 (t, ^3J = 7.5 Hz, 1H), 7.372 (m, 2H), 4.205 (m, 2H), 4.132 (m, 2H), 4.077 (t, ^3J = 7.5 Hz, 2H), 2.568 (m, 2H), 2.200 (m, 2H), 2.032 (m, 2H), 1.854 (br, 2H), 1.648 (m, 2H), 1.348 (m, 2H), 1.278 (m, 2H), 1.199 (m, 4H), 0.803 (t, ^3J = 7.1 Hz, 3H); ^{13}C NMR (125 MHz, $C_2D_4Cl_2$): δ 173.10 (C═O), 162.55 (2 × C═O, imide), 162.52 (2 × C═O, imide), 151.63, 151.51, 151.32, 151.18, 150.39, 150.23, 150.14, 149.99, 148.84, 148.56, 148.21, 148.12, 148.09, 147.94, 147.78, 147.60, 147.58, 147.30, 147.23, 146.56, 146.16, 145.92,145.69, 145.46, 145.24, 145.11, 145.05, 145.03, 144.96, 144.92, 144.86, 144.82, 144.79, 144.74, 144.69, 144.65, 144.60, 144.50, 144.44, 144.26, 144.15, 144.06, 144.04, 143.86, 143.75, 143.72, 143.45, 143.34, 143.30, 143.28, 143.22, 143.04, 143.00, 142.91, 142.81, 142.75, 142.73, 142.70, 142.59, 142.49, 142.41,142.36, 142.26, 142.24, 142.19, 142.10, 142.04, 142.02, 141.97, 141.87, 141.84, 141.81, 141.80, 141.65, 141.63, 141.20, 140.74, 140.59, 140.57, 140.55, 140.52, 140.48, 140.41, 140.33, 140.00, 139.91, 139.89, 139.85, 139.73, 139.71, 139.70, 139.35, 139.29, 139.24, 139.14, 139.04, 139.00, 138.23, 137.85, 135.83, 135.76, 135.71, 135.58, 135.51, 135.48, 135.40, 135.18, 135.04, 134.97, 134.85, 134.73, 134.69, 134.58, 134.55, 134.51, 134.39, 134.29, 133.41 (*CH* of PDI), 133.28 (*CH* of PDI), 131.54, 131.50, 129.66 (*ph*), 129.56 (*ph*), 128.98, 128.90 (*ph*), 128.80 (*ph*), 128.72, 128.69 (*ph*), 128.66, 127.94, 127.87, 126.90, 126.88, 126.81, 126.51, 126.21, 125.03, 124.94, 124.88, 124.78, 123.58, 123.55, 123.13, 97.85, 97.68, 95.09, 94.87, 62.95, 51.58 (spiro *C*), 41.42, 39.29, 38.44, 34.36, 32.17, 30.06, 29.70, 29.57, 28.46, 27.46, 23.05, 20.09, 14.61; MALDI-TOF MS (positive mode, TPB as matrix): *m*/*z*: calcd for $Lu_3C_{126}H_{38}O_6N_3Cl_4$: 2355.97 (100% intensity); found: 2358 $[M + 2H]^{2+}$.

Synthesis of Conjugate 2. Compound **9** (7.3 mg, 7 μmol) and NaOMe (0.8 mg, 0.015 mmol) were dissolved in pyridine (0.5 mL) and stirred for 30 min at 65 °C under N_2. Then, C_{60} (6.5 mg, 0.009 mmol) in 4 mL *o*-DCB was added in. The mixture was stirred at 75 °C for 18 h under N_2. The reaction mixture was separated by HPLC (5PBB column, toluene); the second fraction is the mixture of (5,6)- and (6,6)-monoadducts. By recycling this fraction on a Buckyprep column, the (5,6)- and (6,6)-isomers (**3** and **2**) can be isolated from each other. (5,6)-isomer (**3**) can be converted to (6,6)-isomer (**2**) by a thermal treatment (150−160 °C in *o*-DCB for 5−6 h). Total Yield: 3.2 mg, 88% based on consumed C_{60}; dyad **2**; ^{1}H NMR (500 MHz, $CDCl_3$): δ 8.68 (s, 2H), 8.66 (s, 2H), 7.91 (d, ^2J = 7.3 Hz, 2H), 7.53 (t, ^3J = 7.5 Hz, 2H), 7.46 (t, ^3J = 7.1 Hz, 1H), 4.33 (m, 2H), 4.22 (m, 4H), 2.82 (m, 2 H), 2.42 (m, 2 H), 2.13 (m, 2 H), 1.74 (m, 2 H), 1.44 (m, 2H), 1.37 (m, 2 H), 1.29 (m, 6H), 0.88 (t, ^3J = 6.8 Hz, 3H); ^{13}C NMR (125 MHz, $CDCl_3$): δ 172.81 (C═O), 162.20 (4 × C═O, imide), 148.73, 148.71, 147.75, 147.70, 145.77, 145.74, 145.07, 144.99, 144.97, 144.82, 144.78, 144.71, 144.62, 144.42, 144.38, 144.19, 144.11, 143.92, 143.67, 143.51, 143.46, 142.93, 142.88, 142.81, 142.79, 142.72, 142.71, 142.12, 142.10, 142.04, 142.02, 141.97, 141.90, 141.88, 140.80, 140.71, 140.68, 140.64, 137.82, 137.49, 137.48, 136.61, 135.51, 135.41, 133.11 (*CH* of PDI), 132.97 (*CH* of PDI), 132.09 (*ph*), 131.40, 131.37, 128.76, 128.42, 128.41 (*ph*), 128.23 (*ph*), 123.26, 123.30, 123.27, 122.95, 79.81, 79.76, 62.32, 51.73 (spiro *C*), 41.02, 37.93, 34.01, 33.44, 29.70, 29.32, 29.21, 28.14, 27.30, 27.09, 22.67, 22.25, 14.14; MALDI-TOF MS (negative mode, TPB as matrix): *m*/*z*: calcd for $C_{106}H_{38}O_6N_2Cl_4$: 1576.15 (100% intensity); found: 1576 $[M]^-$.

Synthesis of Compound 9. See Supporting Information.

Theoretical Calculations. The calculations were carried out using the hybrid density functional theory (DFT) at the M06-2X level[12] as implemented in the *Gaussian09* software package.[15] The SDD basis set[15] with the relativistic effective core potential was employed for Lu, 3-21G basis set for C, H, O, N, and 3-21G* for Cl (M06-2X/3-21G~SDD).[13,14]

■ ASSOCIATED CONTENT

Ⓢ Supporting Information

Experimental details including the reaction schemes, synthesis of other compounds, HPLC profiles, mass spectra, CV, DPV curves, 1D and 2D NMR spectra, NMR chemical shifts, DFT-optimized structures of **1** and **2**, transient absorption spectra of **2** and **1**; complete ref 15. This material is available free of charge via the Internet at http://pubs.acs.org.

■ AUTHOR INFORMATION

Corresponding Author

akasaka@tara.tsukuba.ac.jp (T.A.); dirk.guldi@chemie.uni.erlangen.de (D.G.)

Notes

The authors declare no competing financial interest.

■ ACKNOWLEDGMENTS

This work was supported in part by a Grant-in-Aid for Scientific research on Innovative Areas (No. 20108001, "pi-Space"), a Grant-in-Aid for Scientific Research (A) (No. 20245006), The Next Generation Super Computing Project (Nanoscience Project) and Specially Promoted Research (No. 22000009), Nanotechnology Support Project, and Grants-in-Aid for Scientific research on Priority Area (Nos. 20036008, 20038007), and Specially Promoted Research from the Ministry of Education, Culture, Sports, Science, and Technology of Japan. The Strategic Japanese-Spanish Cooperative Program funded by JST and MICINN (fullsol@r PLE2009-0039; Endosol@r PIB2010JP00196). We also thank the Ministerio de Ciencia e Innovación (MICINN) of Spain (Projects CTQ2008-00795/BQU; Consolider-Ingenio CSD2007-00010) and the CAM (MADRISOLAR-2 Project S2009/PPQ-1533). Financial support by the Deutsche Forschungsgemeinschaft through grant no. GU 517/14-1 is gratefully acknowledged.

■ REFERENCES

(1) (a) Martín, N.; Sánchez, L.; Illescas, B.; Pérez, I. *Chem. Rev.* **1998**, *98*, 2527. (b) Bendikov, M.; Wudl, F.; Perepichka, D. F. *Chem. Rev.* **2004**, *104*, 4891. (c) Delgado, J. L.; Bouit, P.-A.; Filippone, S.; Herranz, M. Á.; Martín, N. *Chem. Commun.* **2010**, 4853. (d) Brabec, C. J.; Gowrisanker, S.; Halls, J. J. M.; Laird, D.; Jia, S.; Williams, S. P. *Adv. Mater.* **2010**, *22*, 3839.

(2) (a) Guldi, D. M. *Chem. Commun.* **2000**, 321. (b) Guldi, D. M. *Chem. Soc. Rev.* **2002**, *31*, 22. (c) Bottari, G.; Torre, G.; Guldi, D. M.; Torres, T. *Chem. Rev.* **2010**, *110*, 6768.

(3) (a) Imahori, H.; Hagiwara, K.; Akiyama, T.; Aoki, M.; Taniguchi, S.; Okada, T.; Shirakawa, M.; Sakata, Y. *Chem. Phys. Lett.* **1996**, *263*, 545. (b) Echegoyen, L.; Echegoyen, L. E. *Acc. Chem. Res.* **1998**, *31*, 593. (c) Guldi, D. M.; Prato, M. *Acc. Chem. Res.* **2000**, *33*, 695.

(4) (a) Xie, Q.; Arias, F.; Echegoyen, L. *J. Am. Chem. Soc.* **1993**, *115*, 9818. (b) Reed, C. A.; Bolskar, R. D. *Chem. Rev.* **2000**, *100*, 1075.

(5) (a) Reed, C. A.; Kim, K.-C.; Bolskar, R. D.; Mueller, L. J. *Science* **2000**, *289*, 101. (b) Fujitsuka, M.; Watanabe, A.; Ito, O.; Yamamoto, K.; Funasaka, H. *J. Phys. Chem. A* **1997**, *101*, 7960. (c) Fukuzumi, S.; Mori, H.; Imahori, H.; Suenobu, T.; Araki, Y.; Ito, O.; Kadish, K. M. J. *J. Am. Chem. Soc.* **2001**, *123*, 12458. (d) Ohkubo, K.; Ortiz, J.; Martin-Gomis, L.; Fernández-Lázaro, F.; Sastre-Santos, Á.; Fukuzumi, S. *Chem. Commun.* **2007**, 589.

(6) (a) Shinohara, H. *Rep. Prog. Phys.* **2000**, *63*, 843. (b) Endofullerenes: *A New Family of Carbon Clusters*; Akasaka, T., Nagase, S., Eds.; Kluwer: Dordrecht, The Netherlands, 2002. (c) *Chemistry of Nanocarbons*; Akasaka, T., Wudl, F., Nagase, S., Eds.; John Wiley & Sons: Chichester, 2010. (d) Feng, L.; Akasaka, T.; Nagase, S. Endohedrals. In *Carbon Nanotubes and Related Structures*;

Guldi, D. M., Martin, N., Eds.; John Wiley & Sons: Weinheim, 2010; pp 455−490. (e) Lu, X.; Akasaka, T.; Nagase, S. Rare Earth Metals Trapped inside Fullerenes−Endohedral Metallofullerenes. In *Rare Earth Coordination Chemistry: Fundamentals and Applications*; Huang, C. H., Eds.; John Wiley & Sons: Singapore, 2010; pp 273−308.
(7) (a) Chaur, M. N.; Melin, F.; Ortiz, A. L.; Echegoyen, L. *Angew. Chem., Int. Ed.* **2009**, *48*, 7514. (b) Lu, X.; Akasaka, T.; Nagase, S. *Chem. Commun* **2011**, *47*, 5942.
(8) (a) Rudolf, M.; Wolfrum, S.; Guldi, D. M.; Feng, L.; Tsuchiya, T.; Akasaka, T.; Echegoyen, L. *Chem. Eur. J.* **2012**, *18*, 5136. (b) Takano, Y.; Herranz, Á.; Martín, N.; Radhakrishnan, S. G.; Guldi, D. M.; Tsuchiya, T.; Nagase, S.; Akasaka, T. *J. Am. Chem. Soc.* **2010**, *132*, 8048. (c) Guldi, D. M.; Feng, L.; Radhakrishnan, S. G.; Nikawa, H.; Yamada, M.; Mizorogi, N.; Tsuchiya, T.; Akasaka, T.; Nagase, S.; Herranz, Á.; Martín, N. *J. Am. Chem. Soc.* **2010**, *132*, 9078. (d) Feng, L.; Radhakrishnan, S. G.; Mizorogi, N.; Slanina, Z.; Nikawa, H.; Tsuchiya, T.; Akasaka, T.; Nagase, S.; Martín, N.; Guldi, D. M. *J. Am. Chem. Soc.* **2011**, *133*, 7608.
(9) (a) Pinzón, J. R.; Plonska-Brzezinska, M. E.; Cardona, C. M.; Athans, A. J.; Gayathri, S. S.; Guldi, D. M.; Herranz, M. A.; Martín, N.; Torres, T.; Echegoyen, L. *Angew. Chem., Int. Ed.* **2008**, *47*, 4173. (b) Pinzón, J. R.; Gasca, D. C.; Sankaranarayanan, S. G.; Bottari, G.; Torres, T.; Guldi, D. M.; Echegoyen, L. *J. Am. Chem. Soc.* **2009**, *131*, 7727. (c) Ross, R. B.; Cardona, C. M.; Guldi, D. M.; Sankaranarayanan, S. G.; Reese, M. O.; Kopidakis, N.; Peet, J.; Walker, B.; Bazan, G. C.; Van Keuren, E.; Holloway, B. C.; Drees, M. *Nat. Mater.* **2009**, *8*, 208. (d) Ross, R. B.; Cardona, C. M.; Swain, F. B.; Guldi, D. M.; Sankaranarayanan, S. G.; Van Keuren, E.; Holloway, B. C.; Drees, M. *Adv. Funct. Mater.* **2009**, *19*, 2332.
(10) Grimm, B.; Schornbaum, J.; Cardona, C. M.; van Paauwe, J. D.; Boyd, P. D. W.; Guldi, D. M. *Chem. Sci.* **2011**, *2*, 1530.
(11) (a) Huang, C.; Barlow, S.; Marder, S. R. *J. Org. Chem.* **2011**, *76*, 2386. (b) Li, C.; Wonneberger, H. *Adv. Mater.* **2012**, *24*, 613.
(12) Zhao, Y.; Truhlar, D. G. *Theor. Chem. Acc.* **2008**, *120*, 215.
(13) (a) Binkley, J. S.; Pople, J. A.; Hehre, W. J. *J. Am. Chem. Soc.* **1980**, *102*, 939. (b) Gordon, M. S.; Binkley, J. S.; Pople, J. A.; Pietro, W. J.; Hehre, W. J. *J. Am. Chem. Soc.* **1982**, *104*, 2797.
(14) Cao, X. Y.; Dolg, M. *J. Mol. Struct. (THEOCHEM)* **2002**, *581*, 139.
(15) Frisch, M. J.; et al. *Gaussian09*, Revision A02; Gaussian Inc.: Wallingford, CT, 2009.
(16) Baffeau, J.; Leroy-Lhez, S.; Anh, N.; Williams, R. M.; Hudhomme, P. *Chem.—Eur. J.* **2008**, *14*, 4974.
(17) We assume that stimulated PDI fluorescence is the origin of this feature.
(18) Ehli, C.; Oelsner, C.; Guldi, D. M.; Mateo-Alonso, A.; Prato, M.; Schmidt, C.; Backes, C.; Hauke, F.; Hirsch, A. *Nature Chem.* **2009**, *1*, 243.
(19) Troeger, A.; Ledendecker, M.; Margraf, J. T.; Sgobba, V.; Guldi, D. M.; Vieweg, B. F.; Spiecker, E.; Suraru, S.-L.; Würthner, F. *Adv. Energy Mater.* **2012**, *2*, 536.